AERODYNAMIC MODEL OF TRANSPORT AIRPLANE IN EXTENDED ENVELOPE FOR SIMULATION OF UPSET RECOVERY

N.Abramov[1], M.Goman[1], A.Khrabrov[2], E.Kolesnikov[2], M.Sidoruk[2], B.Soemarwoto[3], H.Smaili[3]
[1] De Montfort University, Leicester, UK
[2]Central Aerohydrodynamic Institute TsAGI, Russia
[3]National Aerospace Laboratory NLR, the Netherlands
mgoman@dmu.ac.uk; khrabrov@postman.ru; Bambang.Soemarwoto@nlr.hl

Keywords: *stall, upset recovery, piloted simulation*

Abstract

The paper presents the aerodynamic model in extended flight envelope for a generic airliner with under wing engines and conventional tail developed within the EU Framework Programme (FP7) research project Simulation of Upset Recovery in Aviation (SUPRA) (www.supra.aero). The SUPRA aerodynamic model is covering angles of attack beyond stall and speeds from take-off to cruise flight. The aerodynamic model in extended flight envelope developed for piloted simulation of upset prevention and recovery has been successfully validated by a number of expert pilots.

1 Introduction

Flight safety of modern transport aircraft is continuously improving due to advanced aircraft design, navigation aids and flight control instrumentation. Nevertheless, various trigger factors such as severe weather conditions, system/component failure or malfunction, pilot's error can lead to flight safety critical situations. The "loss-of-control in-flight" (LOC-I) is now forming the major cause of fatal accidents in public transport operations. LOC-I happens due to a lack of pilot upset situation awareness when aircraft is significantly deviated from the normal flight path. During upset aircraft can reach critical angles of attack when flow separation negatively affects aircraft flight performance, stability and control characteristics potentially leading to LOC-I and failure to safely recover aircraft.

The danger of upset or "unusual attitude" for flight safety was effectively addressed in [1], where an excellent academic and physical background for the problem was presented. A large number of flight accidents have been attributed to a lack of the pilot's awareness and experience in such extreme flight conditions. The need and importance of special pilot training for upset prevention and recovery is now widely recognized by commercial airplane manufacturers, airline companies and flight safety organizations. The requirements for pilot training on modern flight simulators for practicing upset prevention and recovery techniques is now on agenda of the Royal Aeronautical Society's ICATEE (International Committee for Aviation Training in Extended Envelopes http://icatee.org/). It is expected that ICATEE will provide recommendations for enhancing and making better use of current-technology full flight simulators (FFS). The enhancement of FFS assumes that airliner aerodynamic models used in flight simulation should be adequately extended beyond the normal flight envelope boundaries. The current FFS aerodynamic models are systematically validated in the normal flight envelope with limited variation of motion parameters, but in situations when motion parameters exceed these

boundaries a negative training effect may be produced during piloted simulation.

This paper presents the aerodynamic model developed within the EU FP7 project SUPRA aiming for enhanced *representative* aerodynamic modeling, improved piloted stimulation in extended flight envelope and stall recovery training. The experimental and computational techniques and methods earlier validated for military aircraft are applied for an airliner configuration.

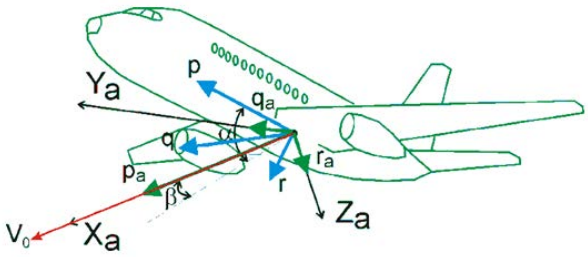

Fig. 1 SUPRA generic airplane configuration.

The backbone for the SUPRA aerodynamic model includes the experimental wind tunnel data obtained in TsAGI for a generic airliner with a low wing two engines with conventional tail configuration (Fig. 1). These aerodynamic data were obtained in low speed and transonic wind tunnels using different experimental facilities. Additional aerodynamic data for a T-tail aircraft configuration were generated at NLR using CFD methods. The basic aircraft geometry for CFD study was derived from the NACRE model (New Aircraft Concepts REsearch) which was developed in the EU FP-6 NACRE project (2005-2009).

The basic requirement for the aerodynamic data means that they should reflect generic nonlinear aerodynamic phenomena at high angles of attack and be representative in a sense that pilots can be exposed to various aircraft dynamic behaviours associated with instability and loss of control due to stall and flow separation. The following sections present how the experimental and computational data are processed, reconciled and validated for integration in the SUPRA representative aerodynamic model.

2 Upset recovery scenarios

Analysis of upset-related flight accidents shows that upset events may advance through different phases dynamically evolving from safe ones to critically dangerous [2]. This is illustrated in Fig. 2. Upsets are usually associated with unusual attitudes with pitch and bank angles exceeding normally encountered in flight operations of transport aircraft. The aircraft may be still within the normal aerodynamic model flight envelope and aircraft remains controllable with potential for successful recovery. The pilot should just overcome his standard stereotypes in pitch and roll control and act in an adequate manner. In case of incorrect recovery an unusual attitude can evolve into stall or situation when aircraft exceeds speed or g-limits. Both these situations being critically dangerous require special pilot training. Based on this analysis the requirements for the aerodynamic model become clear. The normal flight envelope, where FFS aerodynamic models are well validated should be extended to areas with high angles of attack at low and high Mach numbers from take-off to cruise speeds of flight.

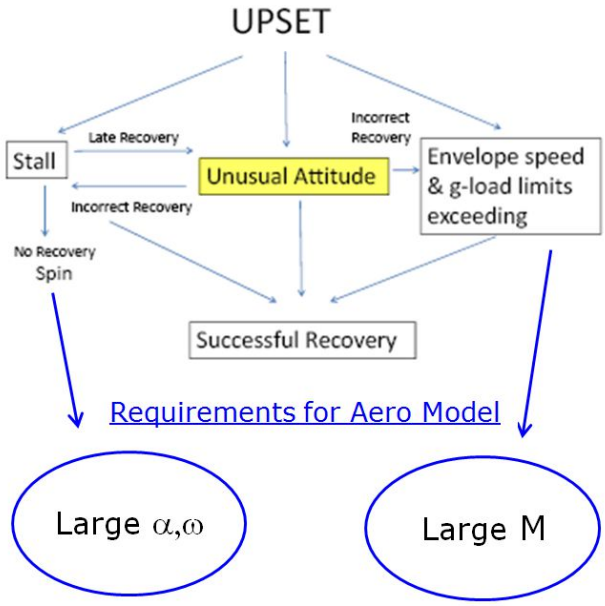

Fig. 2 Upset conditions and requirements for extended aerodynamic model [2].

3 Aerodynamic model in extended envelope

The aerodynamic model of a generic airplane configuration with under-wing engines and conventional tail is developed for a wide range of angles of attack, sideslip and angular rate based on experimental data obtained in TsAGI's wind tunnels using static, forced oscillations and rotary balance tests. Mach dependence for aerodynamic coefficients is tested in wind tunnel in the limited range of angles of attack (static tests, free-oscillations with small amplitudes, see yellow area in Fig. 3). Opposite, a wide range of angles of attack, sideslip ($-20<\alpha<90$ deg, $|\beta|<30$ deg), and rate of rotation (forced oscillation tests with small and large amplitudes, rotary balance tests) can be investigated only for low Mach numbers (blue area in Fig. 3). Special procedures for combining available data obtained on different experimental facilities are required to allow the aerodynamic model in extended flight envelop to be smooth, consistent and valid in a wider region of flight parameters, for example in the corner area between blue and yellow regions, where stall is still possible within allowable structural limits.

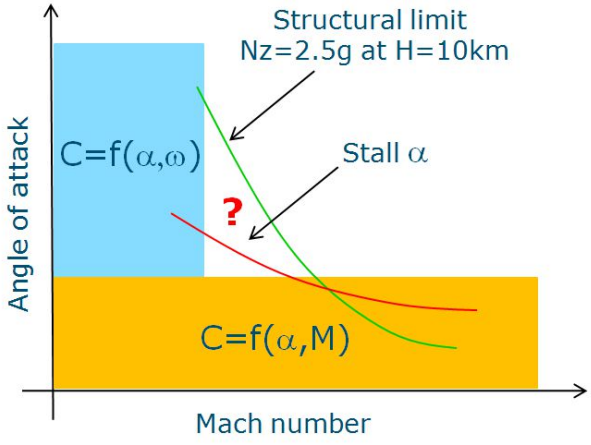

Fig. 3 Areas of aerodynamic wind tunnel data.

3.1 Key aerodynamic phenomena at stall

Increase of angle of attack above some critical value leads to stall which is associated with onset of flow separation over an area of the wing [3,5,6,15]. A sudden loss of lift at/near the stall and nonlinear transformation in the pitching moment coefficient are typical consequences of flow separation (Fig. 4). Stall conditions may also produce strong dependence of the aerodynamic loads on prehistory of motion. Fig. 5 shows variation in the normal force coefficient in static conditions (filled circles) and during forced oscillations with a number of non-dimensional frequencies k at large amplitude of oscillations (empty markers). One can see significant difference in the normal force during increase and decrease of angle attack. Such dynamic hysteresis can produce negative damping in the pitching moment (Fig. 6). A number of nonlinear dynamics effects can occur due to these phenomena such as g-break and altitude loss, dynamic instability, pitch-up departure and deep stall regime.

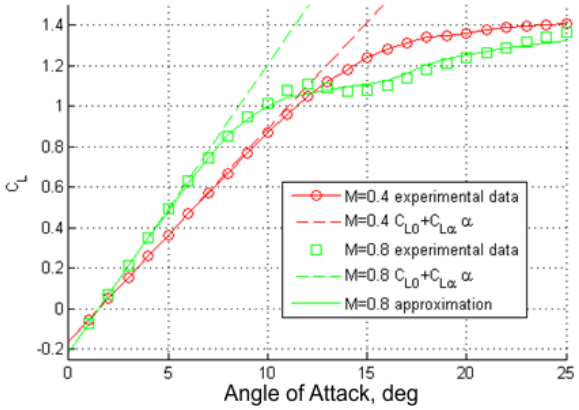

Fig. 4 Lift coefficeint vs angle of attack and Mach number.

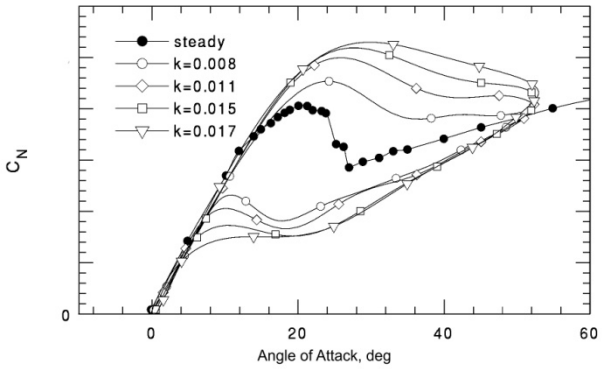

Fig. 5 Normal force at stall/beyond stall conditions: static (filled circles) and dynamic dependencies (empty markers).

In the lateral/directional mode stall leads to deterioration of the rolling and yawing moment

coefficients negatively affecting airplane stability and control effectiveness. Figs. 7 (static test) and 8 (rotary balance test) show dependences of the rolling and yawing moment coefficients on angle of attack sideslip and non-dimensional rate of rotation ω (note that ω is equivalent to p_a shown in Fig. 1).

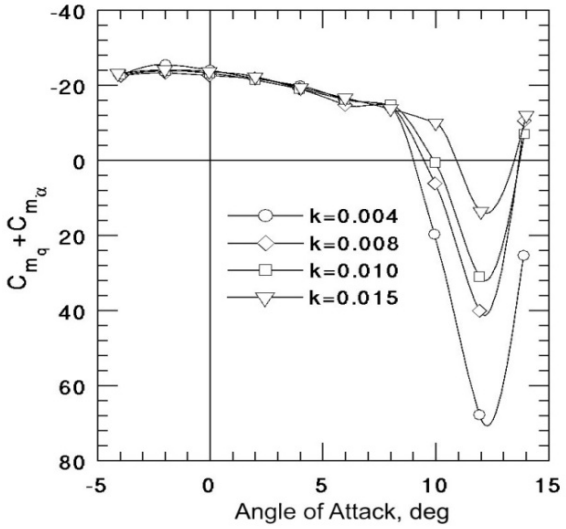

Fig. 6 Negative damping in the pitching moment.

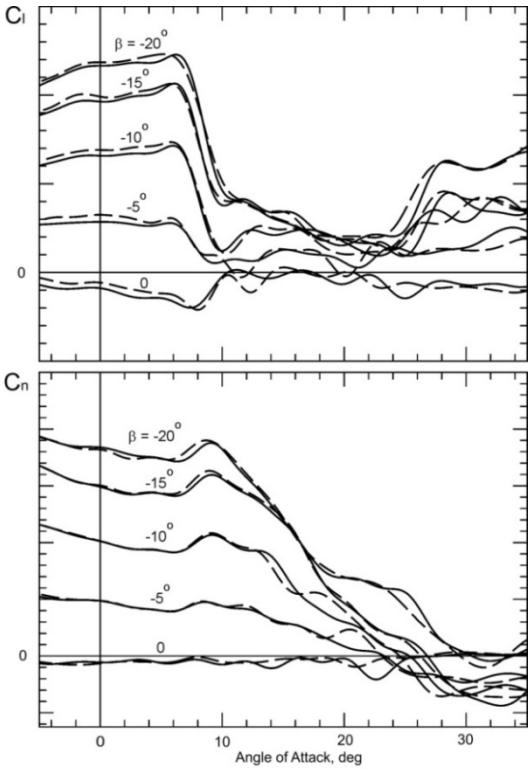

Fig. 7 Rolling and yawing aerodynamic moments vs angle of attack and sideslip.

Note that onset of directional instability $C_{n\beta} < 0$ at $30 < \alpha < 50^0$ is due to vertical tail shadowing by fuselage and wing.

3.1.1 Analytic approximations

Multidimensional dependencies of aerodynamic coefficients obtained in rotary balance (RB) tests and represented in the form of look-up data tables is convenient to approximate by the polynomial expansion ($i = X, Y, Z, l, m, n$)

$$C_{i\,\mathrm{RB}}(\alpha,\beta,\omega) = C_{i0}(\alpha) + C_{i\beta}(\alpha)\beta + C_{i\omega}(\alpha)\omega + C_{i\beta\omega}(\alpha)\beta\omega + C_{i\beta^2}(\alpha)\beta^2 + C_{i\omega^2}(\alpha)\omega^2 + C_{i\beta\omega}(\alpha)\beta\omega + C_{i\beta^3}(\alpha)\beta^3 + C_{i\beta^2\omega}(\alpha)\beta^2\omega + C_{i\beta\omega^2}(\alpha)\beta\omega^2 + C_{i\omega^3}(\alpha)\omega^3 \quad (1)$$

which helps to separate the aerodynamic asymmetry, aerodynamic autorotation and nonlinear terms. Accuracy of this approximation is shown in Fig. 8 (solid lines - experimental data, dashed lines - polynomial expansion).

To accommodate the outlined aerodynamic effects in the aerodynamic model wind axes projections of angular velocity p_a, q_a, r_a are used instead of body axes angular rates p, q, r (see Fig. 1). This allows direct use of aerodynamic dependencies obtained in the rotary balance tests (note that $p_a = \omega$):

$$\begin{aligned} p_a &= p\cos\alpha\cos\beta + r\sin\alpha\cos\beta + q\sin\beta \\ r_a &= p\sin\alpha - r\cos\alpha \\ q_a &= -p\cos\alpha\sin\beta - r\sin\alpha\sin\beta + q\cos\beta. \end{aligned} \quad (2)$$

The following assembly of the aerodynamic model is applied using the aerodynamic data from static (ST), forced oscillation (FO) and rotary balance (RB) tests ($i = X, Y, Z, l, m, n$)

$$C_i = C_{i\,\mathrm{ST}}(\alpha,\beta) + \Delta C_{i\,\mathrm{RB}}(\alpha,\beta,p_a) + \Delta C_{i\,\mathrm{ST}}(\alpha,\delta) + C_{i\,q_aFO}(\alpha)q_a + C_{i\,r_aFO}(\alpha)r_a \quad (3)$$

Aerodynamic derivatives in (3) with respect to q_a and r_a angular rates are calculated from the aerodynamic derivatives obtained in forced oscillation tests with respect to body axis angular rates p, q, r.

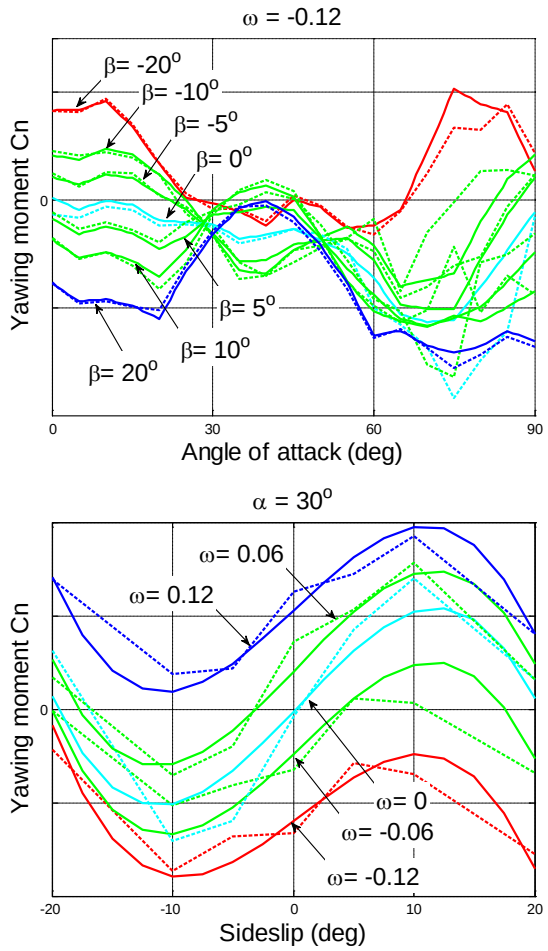

Fig. 8 Yawing moment coefficient vs angle of attack, sideslip and nondimensional rate of rotation.

To extrapolate the aerodynamic dependencies on Mach number to higher angles of attack (the yellow region in Fig. 3) the following functional approximation is used (the lift coefficient is considered as an example):

$$C_L(\alpha, M) = C_{L0}(M) + k_1(M) \cdot C_{L(M=0.4)}\left(k_2(M) \cdot \alpha\right) \quad (4)$$

where $C_{L0}(M)$ is the dependence of the lift coefficient at zero incidence, $C_{L(M=0.4)}(\alpha)$ is the experimental dependence of the lift coefficient at M=0.4, $k_1(M)$ and $k_2(M)$ are identified to approximate experimental dependencies at different Mach numbers. In fact, only coefficient $k_1(M)$ should be identified since $k_1(M)$ and $k_2(M)$ are not independent:

$$k_1(M) = \frac{C_{L\alpha}(M)}{C_{L\alpha}(M = 0.4) \cdot k_2(M)} \quad (5)$$

The accuracy of approximation (5) is shown in Fig. 4. Decoupling functional approximation for Mach number and angle of attack dependencies similar to (4) and (5) are applied in the SUPRA extended aerodynamic model for all longitudinal and lateral/directional aerodynamic coefficients.

3.1.2 Unsteady aerodynamics model

Unsteady aerodynamic effects at stalled conditions require implementation of special modelling approach [6,7]. The unsteady aerodynamic contribution may be represented as additional aerodynamic term in (3), for example, as follows

$$C = C(\alpha, \delta) + C_{dyn}(t) \quad (6)$$

where the time dependent component in (6) is described by the ordinary differential equation shown below as a washout filter

$$C_{dyn} = \frac{\tau s}{\tau s + 1} \Delta C(\alpha) \quad (7)$$

Note that in static conditions term C_{dyn} gives zero contribution to the total aerodynamic load. The SUPRA aerodynamic model incorporates unsteady nonlinear variations of type (7) in the lift and pitching moment coefficients.

3.1.3 Reynolds number effects

The most significant issue involved in using wind tunnel aerodynamic data for simulation of airplane dynamics at stall conditions is the discrepancy in values of Reynolds number between the wind tunnel model ($\mathrm{Re} \approx 1.0 * 10^6$) and full-scale airplane ($\mathrm{Re} \approx 20 * 10^6$). Separated flow conditions may be significantly affected by Reynolds number. As Reynolds number increases from model conditions to the full-scale value significant increases in the magnitude and angle of attack for maximum lift take place. Normally the variation of lift with angle of attack is negative immediately beyond maximum lift. In free flight the down-going

wing will experience a loss of lift, further increasing the tendency for the wing to drop and resulting in a pro-spin propelling rolling moment known as wing autorotation. An intensity of aerodynamic autorotation and angle of attack range where it takes place similarly to the lift case should strongly depend on Reynolds number. As a result the prediction of airplane flight characteristics near and above stall will strongly depend on Reynolds number effect. One can expect that increase in Reynolds number at full-scale airplane will lead to more intensive post-stall departure, more dangerous spin at higher angles of attack and unsatisfactory spin recovery [8].

3.2 Complementary use of CFD

The SUPRA aerodynamic model developed based on experimental wind tunnel data includes a number of reconfigurable parameters. They need to be tuned to produce a representative airplane behavior at stall and beyond stall conditions, which will be positively accepted by expert pilots. CFD capabilities available at NLR were used for evaluation of Reynolds effects on dynamic stall, aerodynamic autorotation and onset of asymmetry. These results allowed to tune the SUPRA model reconfigurable parameters within in justifiable physical limits.

3.2.1 CFD method

NLR's CFD solver ENSOLV is employed as the CFD method [9]. ENSOLV is based on a multi-block structured grid to give the solution of the Navier-Stokes equations. There are two modes involved in the present investigation, namely the Reynolds-Averaged Navier-Stokes (RANS) mode and the hybrid RANS/LES mode (Large Eddy Simulation). In the RANS mode, the Turbulence Numerics Team (TNT) formulation of the k–ω turbulence model is applied [10].

In the hybrid RANS/LES mode, the X-LES [11] formulation is applied. X-LES is a particular DES method [12] that consists of a composition of a RANS k–ω turbulence model and a k-equation SGS model. Both the RANS k–ω model and the k-equation SGS model use the Boussinesq hypothesis to model the Reynolds or subgrid-scale stress tensor, which depends on the eddy-viscosity coefficient ν_t. Both models are based on the equation for the modelled turbulent kinetic energy k, which depends on its dissipation rate ε. Both the eddy viscosity and the dissipation rate are modelled using the turbulent kinetic energy as velocity scale together with a length scale l_t,

$$\nu_t = l_t\sqrt{k} \qquad \text{and} \qquad \varepsilon = \beta_k \frac{k^{3/2}}{l_t},$$

where l_t is defined as a combination of the RANS length scale $l = \sqrt{k}/\omega$ and the SGS filter width Δ,

$$l_t = \min\{l, C_1\Delta\}$$

with C_1 = 0.05. The RANS k–ω model is completed by an equation for the specific dissipation rate ω and uses the TNT set of coefficients. The X-LES method will be in LES mode when the filter width (times C_1) is small compared to the RANS length scale. Note that in that case the SGS model is completely independent of ω.

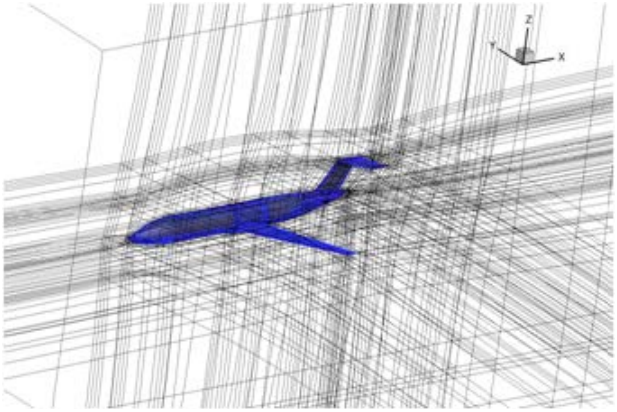

Fig. 9 NACRE model geometry and CFD grid.

3.2.2 Geometry and grid

The baseline T-tail configuration of the NACRE aircraft [13] is used as a means to generate the high angles of attack flow phenomena. Fig. 9 gives an illustration of the aircraft geometry and implemented grid. A multi-block structured grid is generated around the complete aircraft configuration. For affordability, the so-called medium grid resolution consisting of about 4.2 million cells is used to generate the flow

solutions. The grid is appropriately stretched towards the solid wall to sufficiently resolve the boundary layer by the value of y+ of around unity. Fig. 10 shows examples of flow visualisation for separated from the wing wake interacting with T-tail for two different angles of attack.

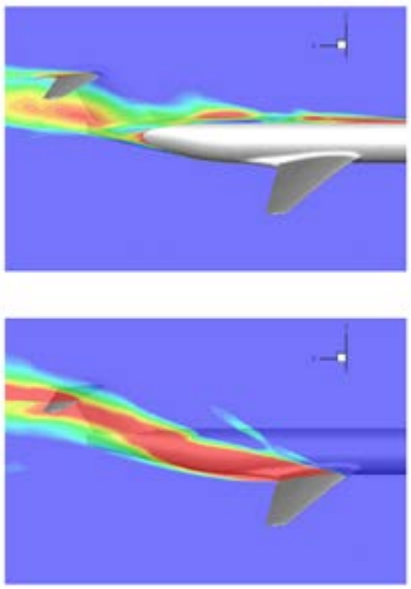

Fig. 10 Flow visualization showing wind tail interaction.

3.2.3 Autorotation

Assessment of the autorotation characteristics can be conducted through coning motions at varying roll-rate. Two approaches have been used. The first approach employs a time-accurate simulation, where a time-averaged force and moment coefficients are obtained by averaging the time-accurate data. The second approach is an approximate one, using a steady-state simulation. In the latter case, the force and moment coefficients are obtained by averaging the alternating values of the force and moment coefficients from a non-converged steady-state solution. Both approaches use the RANS modeling.

Apparently, the second approach is more economical in terms of computational resource. It requires a fraction of CPU time. Although it gives only approximative results, in some cases it can produce the phenomenological trends in a level of approximation that is sufficient for the purpose of aerodynamic modelling.

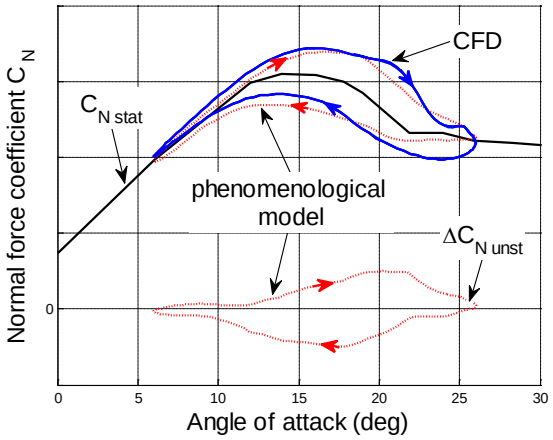

Fig. 11 Phenomenological model vs CFD simulation.

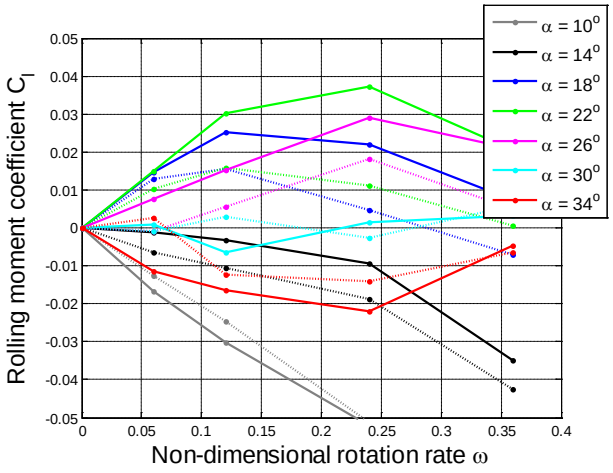

Fig. 12 NACRE model CFD prediction of aerodynamic autorotation in the rolling moment (solid lines Re=20*10^6, dashed lines Re=1*10^6).

CFD modeling results for the normal force in static conditions (black solid line) and at periodical variation of angle of attack $\alpha = 16^0 + 10^0 \sin 2\pi ft$ (blue solid line) with frequency $f = 0.35Hz$ are presented in Fig. 11. This simulation reveals a significant hysteresis loop in variation of the force coefficient. Similar hysteresis loop can be modelled using a phenomenological model of type (6), (7). After identification of the phenomenological model parameters, i.e. the characteristic time constant ($\tau = 0.1\text{sec}$) and nonlinear function $\Delta C(\alpha)$, the

predicted hysteresis loop (red dashed line in Fig. 11) is quite close to the CFD results.

Aerodynamic autorotation for NACRE model was evaluated at two Reynolds numbers corresponding to wind tunnel and full-scale airplane conditions, $Re = 1 * 10^6$ and $Re = 20 * 10^6$, respectively (see Fig. 12). As it was expected, increase in Reynolds number from wind tunnel to full-scale free flight conditions significantly increases the pro-spin autorotation rolling moment C_l. For example, at $\alpha = 22^0$ the maximum magnitude of the pro-spin autorotation approximately two times bigger than it could be observed in wind tunnel.

.3.4 Aerodynamic model validation

For Level D certified Full Flight Simulators (FFS) the model output accurately matches aircraft responses measured in flight. This requirement is valid only for linear systems, which is the case for airplane dynamics in normal flight envelope. Similar validation criterion for post-stall nonlinear airplane dynamics is practically not applicable. Validation of the SUPRA representative aerodynamic model has been conducted through 1) comparison with dynamically scaled free-spinning model in vertical wind tunnel, 2) systematic investigation of SUPRA nonlinear dynamics above stall, 3) piloted simulation with expert pilots.

3.4.1 Comparison with free-flight scaled model

Although Reynolds number may strongly affect aerodynamic characteristics in stall region, it is generally accepted that dynamically scaled free-spinning models in vertical wind tunnel serve as an effective instrument for investigation of spin modes and spin recovery procedures [8].

Comparison of the SUPRA model simulated results with experimental time histories obtained in TsAGI's vertical wind tunnel is shown in Fig. 13 (experimental results - the top two graphs). This comparison indicates quite good qualitative and quantitative agreement in spin mode characteristics and also in the respond to applied spin recovery control.

3.4.2 Computational investigation of SUPRA nonlinear flight mechanics

Airplane dynamics at stall and beyond stall attitudes is highly nonlinear with multiple modes of motion and different types of stability. For validation purposes of SUPRA model a systematic investigation of its nonlinear dynamics in extended envelope has been conducted using computation of all attainable trims or equilibrium states and their local stability characteristics [14].

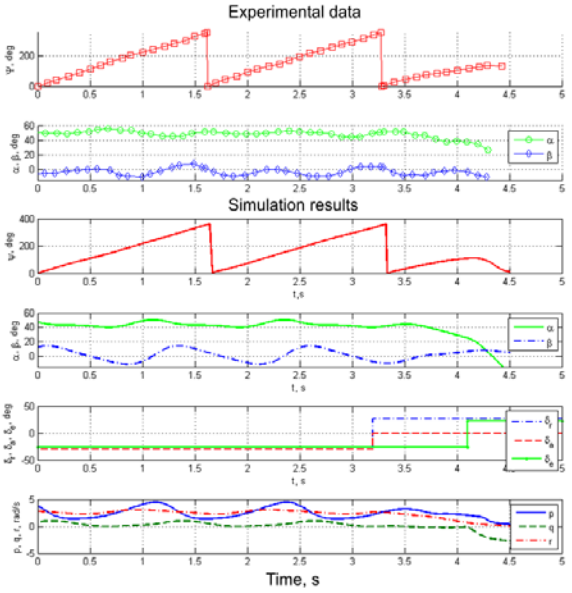

Fig. 13 Experimental and simulation results for spin recovery of dynamically scaled free-flight model in TsAGI verical wind tunnel.

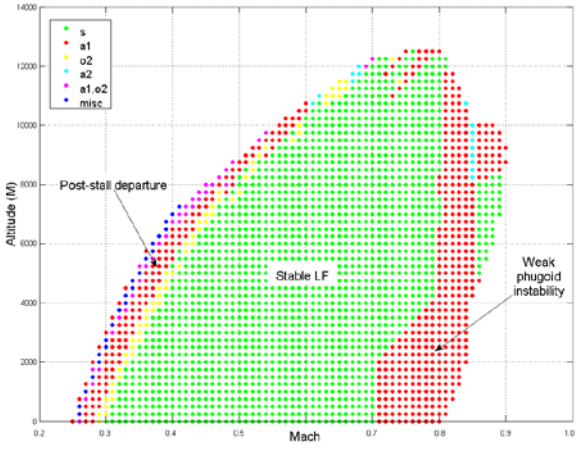

Fig. 14 SUPRA envelope in (H,M) for straight and level flight.

Fig. 14 shows reconstructed flight envelope in (Altitude, Mach) plane for the straight and level flight of SUPRA model indicating SUPRA model performance characteristics. Regions with stable flight, weak phugoid instability and post-stall departure instability are clearly marked.

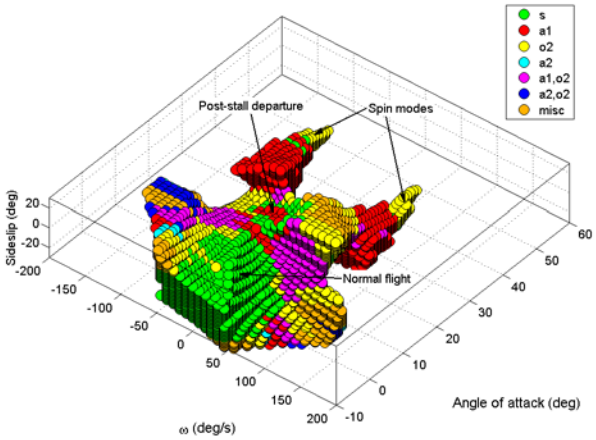

Fig. 15 Manoeuvre envelope; attainable equilibrium set in space of angle of attack, sideslip and rotation rate (α,β,ω).

Manoeuvrability characteristics and critical regimes are analyzed via computation of all attainable trims or equilibria in the space of motion parameters α, β, ω (see Fig. 15). Different colors specify character of equilibrium point stability: green - stable, red - aperiodically unstable, yellow - oscillatory unstable regime, etc.

Investigation of airplane critical regimes such as post-stall departure, post-stall gyration, incipient/developed spin modes is illustrated in Fig. 16.

3.4.3 Piloted validation and parameter tuning

The final stage of SUPRA aerodynamic model validation was made via piloted simulation with participation of a number of experienced test and airline pilots on three flight simulators – Desdemona (TNO), Grace (NLR) and PSPK-102 (TsAGI). Valuable feedback from pilots on representativeness of stall dynamics in qualitative and quantitative terms helped to tune SUPRA model reconfigurable parameters to improve its fidelity. Fig. 17 shows a number of simulated trajectories during post stall departures and excursions to very high angles of attack projected on the plane of angle of attack and sideslip angle. Alpha\Beta envelopes for B757 taken from [1] is given for comparison.

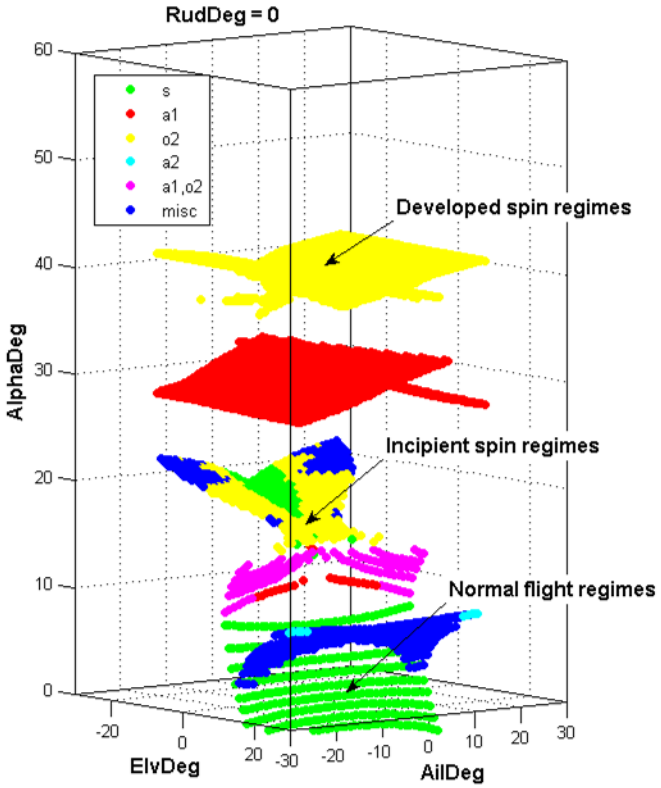

Fig. 16 Equilibrium surfaces for angle of attack in normal and critical flight regimes vs elevator and aileron deflections (green marker - stable, red - aperiodically unstable, yellow - oscillatory unstable regime, etc).

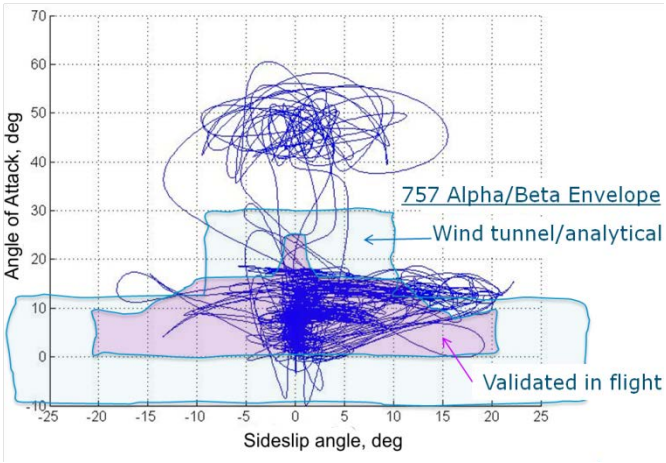

Fig. 17 SUPRA model simulaion: α,β envelope

4 Concluding remarks

- SUPRA generic aerodynamic model allows simulation of multiple phenomena representative for stall/post-stall flight conditions.
- A combination of wind tunnel and CFD data allow reconfiguration of the SUPRA aerodynamic model parameters within justifiable physical limits.
- Validation and tuning of the SUPRA aerodynamic model included systematic computational investigation of nonlinear dynamics in extended flight envelope and simulation with pilots experienced in stall dynamics (V.Birukov, etc.)

Copyright Statement

References

[1] Airplane Upset Recovery Training Aid. Revision 2, November 2008

[2] Biryukov V., Fucke L., Grigoriev M., Groen E., et al. Developing Scenarios for Research into Upset Recovery Simulation AIAA-2010-7794, *AIAA Modeling and Simulation Technologies Conference*, Toronto, ON, 2-5 August 2010.

[3] Foster, J.V., Cunningham, K., Fremaux, Ch.M., Shah, G.H., Stewart, E.C., Rivers, R.A., Wilborn, J.E., Gato, W. Dynamics Modeling and Simulation of Large Transport Airplanes in Upset Conditions. AIAA-2005-5933, *AIAA Atmospheric Flight Mechanics Conference and Exhibit*, 15-18 August 2005, San Francisco, California.

[4] Cunningham, K., Foster, J.V., Shah, G.H., Stewart, E.C., Ventura, R.N., Rivers, R.A., Wilborn, J.E., Gato, W. Simulation Study of Flap Effects on a Commercial Transport Airplane in Upset Conditions. AIAA-2005-5908, *AIAA Atmospheric Flight Mechanics Conference and Exhibit*, 15-18 August 2005, San Francisco, California.

[5] Gingras, D.R. and Ralston, J.N. Improvement of Stall-Regime Aerodynamics Modeling for Aircraft Training Simulations. AIAA-2010-7793, *AIAA Modeling and Simulation Technologies Conference*, Toronto, ON, 2-5 August 2010.

[6] Goman, M.G. and Khrabrov, A.N. State-Space Representation of Aerodynamic Characteristics of an Aircraft at High Angles of Attack. *Journal of Aircraft* 31, (5), pp.1109-1115, 1994.

[7] Khrabrov, A.N., Vinogradov, Yu.N. and Abramov, N.B. Mathematical Modelling of Aircraft Unsteady Aerodynamics at High Incidence with Account of Wing-Tail Interaction, AIAA-2004-5278, *AIAA Atmospheric Flight Mechanics Conference and Exhibit*, Providence, Rhode Island, August 2004.

[8] Chambers, J.R. Modeling Flight: The Role of Dynamically Scaled Free-Flight Models in Support of NASA's Aerospace Programs. NASA SP 2009-575.

[9] Kok, J.C., Boerstoel, J.W., Kassies, A. and Spekreijse, S.P. A Robust Multi-Block Navier-Stokes Flow Solver for Industrial Applications. *Proceedings of ECCOMAS Conference*, Paris, 1996 (also NLR-TP-96323, 1996).

[10] Kok, J.C. Resolving the dependence on freestream values for the κ–ω turbulence model. *AIAA Journal*, 38(7), pp. 1292-1294, 2000.

[11] Kok, J.C., Dol, H.S., Oskam, B. and van der Ven. Extra-large eddy simulation of massively separated flows. AIAA-2004-264, *42nd AIAA Aerospace Sciences Meeting*, Reno, NV, 5–8 January 2004.

[12] Spalart, P.R., Jou, W.-H., Strelets, M. and Allmaras, S.R. (1997) Comments on the feasibility of LES for wings, and on a hybrid RANS/LES approach. *In C.Liu and Z.Liu, Editors, Advances in DNS/LES. Greyden Press. Proc. 1st AFOSR Int. Conf. on DNS/LES*, Ruston (LA), 1997.

[13] Schmollgruber, P. and Jentink, H. A multidisciplinary flying testbed for new aircraft concepts. Proceedings of 27th ICAS Congress, Nice, Sept. 2010, p.6.9.2.

[14] Goman, M.G., Khramtsovsky, A.V. and Kolesnikov, E.N. Evaluation of Aircraft Performance and Maneuverability by Computation of Attainable Equilibrium Sets. *AIAA Journal of Guidance, Control, and Dynamics*, Vol. 31, No. 2, pp. 329-339, 2008.

[15] Abramov, N.B., Goman, M.G., Khrabrov, A.N. and Soemarwoto, B. Aerodynamic Model Development for Simulation of Upset Recovery of Transport Airplane, *RAeS Aerodynamics Conference - Applied Aerodynamics: Capabilities and Future Requirements*, London, 27-28 July 2010.